Directionality and maneuvering effects on a surface ship underwater acoustic signature

Mark V. Trevorrow[a] and Boris Vasiliev
Defence R&D Canada-Atlantic, Dartmouth, Nova Scotia, Canada B2Y 3Z7

Svein Vagle
Fisheries and Oceans Canada, Institute of Ocean Sciences, Sidney, British Columbia, Canada V8L 4B2

(Received 13 February 2008; revised 29 April 2008; accepted 8 May 2008)

This work examines underwater source spectra of a small (560 tons, 40 m length), single-screw oceanographic vessel, focusing on directionality and effects of maneuvers. The measurements utilized a set of four, self-contained buoys with GPS positioning, each recording two calibrated hydrophones with effective acoustic bandwidth from 150 Hz to 5 kHz. In straight, constant-speed runs at speeds up to 6.2 m s^{-1}, the ship source spectra showed spectral levels in reasonable agreement with reference spectra. The broadband source level was observed to increase as approximately speed to the fourth power over the range of 2.6–6.1 m s^{-1}, partially biased at low speeds by nonpropulsion machinery signals. Source directionality patterns were extracted from variations in source spectra while the ship transited past the buoy field. The observed spectral source levels exhibited a broadside maximum, with bow and stern aspect reduced by approximately 12–9 dB, respectively, independent of frequency. An empirical model is proposed assuming that spectral source levels exhibit simultaneous variations in aspect angle, speed, and turn rate. After correction for source directionality and speed during turning maneuvers, an excess of up to 18 dB in one-third octave source levels was observed.
 [DOI: 10.1121/1.2939128]

PACS number(s): 43.30.Nb, 43.30.Jx [RCG] Pages: 767–778

I. INTRODUCTION

The low-frequency underwater acoustic output generated by surface ships is a significant contributor to background ambient noise in the sea. This is especially true in littoral regions, near harbors and shipping lanes. With minimal acoustic attenuation at low frequencies (LFs), ship acoustic footprints can extend significant distances, potentially of the order tens to hundreds of kilometers for LF (<100 Hz) signals. In the civilian domain, concerns regarding acoustic noise pollution arise with the effects of shipping on marine mammals and fisheries. In the naval area, underwater radiated signatures represent a vulnerability for both surface vessels and submarines, and thus these vessels are specifically designed to minimize their acoustic signature over a broad range of frequencies. Additionally, naval vessels are often required to perform aggressive maneuvers, so it is important to understand changes in their acoustic signature during such maneuvers. Although measurement of the broadband acoustic signature from ships is straightforward in principle, there are several subtle features of ship signatures which deserve attention. Specifically, the directionality of vessel radiated signatures and the effects of turning maneuvers are examined in this work.

In this study, the underwater acoustic output from a ship will be called *signature*. As a result of a number of studies since the second World War,[1–4] the general features of a ship's signature are reasonably well known. There are two major components: narrowband propeller and machinery lines, and broadband cavitation, turbulence, and bubble mediated output. Fundamental propeller shaft and blade-rate signals lie in the 1–20 Hz range, dependent on ship and propeller design and speed, with multiple harmonics extending upwards to 100 Hz[3]. Gray and Greeley[5] presented a model for propeller blade-rate signatures, identifying propeller cavitation as the source mechanism. Other narrowband shipboard machinery (e.g., generator and compressor) signals may extend as high as 3 kHz. Broadband propeller cavitation, turbulent flow, and bubble generation sounds extend from roughly 100 Hz upwards, with a spectral level varying approximately as inverse frequency squared.[1] In some literature,[2,4] the ship acoustic signatures have been assumed horizontally omnidirectional. Other recent studies[3] present directivity measurements showing reduced levels at bow and stern aspects.

While a few deep-water acoustic ranges exist (e.g., Atlantic Underwater Test and Evaluation Center—AUTEC, utilized by Arveson and Vendittis[3]), the authors are aware of a number of fixed, shallow-water sound ranges. These shallow-water facilities can be useful for routine stationary or low-speed measurements, particularly for relative measurements, e.g., to assess changes due to differing machinery states. However, such facilities are generally too shallow and close to shore to allow ships to maneuver freely at greater speeds. Air-dropped sonobuoys have been used in some deep-water studies;[4] however, precise positioning of the ship and buoys and precise acoustic calibration remain problem-

[a]Author to whom correspondence should be addressed. Electronic mail: mark.trevorrow@drdc-rddc.gc.ca.

Report Documentation Page

Form Approved
OMB No. 0704-0188

1. REPORT DATE	2. REPORT TYPE	3. DATES COVERED
29 APR 2008		**00-00-2008 to 00-00-2008**

4. TITLE AND SUBTITLE	5a. CONTRACT NUMBER
Directionality and maneuvering effects on a surface ship underwater acoustic signature	5b. GRANT NUMBER
	5c. PROGRAM ELEMENT NUMBER
6. AUTHOR(S)	5d. PROJECT NUMBER
	5e. TASK NUMBER
	5f. WORK UNIT NUMBER
7. PERFORMING ORGANIZATION NAME(S) AND ADDRESS(ES) **Defence R&D Canada-Atlantic,Dartmouth, Nova Scotia, Canada B2Y 3Z7,**	8. PERFORMING ORGANIZATION REPORT NUMBER
9. SPONSORING/MONITORING AGENCY NAME(S) AND ADDRESS(ES)	10. SPONSOR/MONITOR'S ACRONYM(S)
	11. SPONSOR/MONITOR'S REPORT NUMBER(S)

12. DISTRIBUTION/AVAILABILITY STATEMENT
Approved for public release; distribution unlimited

13. SUPPLEMENTARY NOTES

14. ABSTRACT

15. SUBJECT TERMS

16. SECURITY CLASSIFICATION OF:			17. LIMITATION OF ABSTRACT	18. NUMBER OF PAGES	19a. NAME OF RESPONSIBLE PERSON
a. REPORT	b. ABSTRACT	c. THIS PAGE			
unclassified	**unclassified**	**unclassified**	**Same as Report (SAR)**	**12**	

atic. Additionally, measurement of ship signatures at longer ranges often requires a difficult compensation for acoustic propagation effects.[2] In this work, a set of four broadband underwater recording buoys (BURBs) was developed to overcome some of these limitations. In addition to allowing the vessel to maneuver freely well away from shore, operating in deeper waters minimizes or removes seabed interactions, simplifying estimation of the low-frequency source levels.

The BURB system was developed in 2004/2005 through a collaboration between Defence R&D Canada Atlantic and the Institute of Ocean Sciences. This prototype system was intended to demonstrate the concept of a portable acoustic ranging system for the Canadian Navy. The BURBs were designed to provide continuous recording of two calibrated hydrophones, each with 20 kHz bandwidth. Relative positioning of the individual BURBs and the target ship was accomplished through commercially available differential global positioning systems (DGPSs). This work describes the first major sea trial of the BURBs against a small oceanographic vessel (CCGS VECTOR, 39.7 m LOA). While these particular sea trials uncovered some practical limitations in these prototype buoys, an examination of the data uncovered several interesting features of ship signatures. In particular, the ship's acoustic directionality and the increased source levels generated by turning maneuvers were investigated and described herein. A goal of the analysis was to devise a simple, empirical model that could account for the major dependencies in the signature during maneuvers. In particular, signature variations due to frequency, aspect angle, speed, and turn rate were investigated. Section II describes the BURBs and the experimental approach. An important discussion of surface-reflected acoustic multipath effects is presented in Sec. II E. Section III will present an overview of the acoustic results from the three days of sea trials in mid-April 2005. Finally, Sec. IV will present summary discussions and recommendations.

II. EXPERIMENT

A. Broadband underwater recording buoys

The BURBs (see photo in Fig. 1) were developed to provide broadband, short time-scale measurement of vessel underwater radiated signatures. A detailed description of the BURB system is given by Trevorrow *et al.*[6] The BURB system was intended to remedy problems of positioning, calibration, data dynamic range, lifetime, and background noise encountered with the use of conventional sonobuoys. There were four identical BURBs, each completely self-contained with an operational duration in excess of 24 h. Each buoy continuously recorded two hydrophone channels onto an internal hard drive. Each hydrophone channel was sampled at 40 000 samples/s with 16 bit (92 dB) dynamic range.

Additionally, an automatic gain control (AGC) adjusted the recording levels by up to 58 dB. The buoys recorded their own position through an onboard DGPS receiver at 1 s intervals. Each buoy was approximately 110 cm high by 60 cm maximum diameter, with a weight of 45 kg. In these trials, the two hydrophones on each BURB were suspended

FIG. 1. Photograph of a BURB during deployment from the CCGS Vector, April 2005. Inset at lower right shows the hydrophone, cable, strength member, and lead weight.

at depths of 5 and 15 m below the surface package. The hydrophones were inexpensive commercial units approximately 10 cm in length by 2 cm diameter with integral preamplifier. Note that the use of two different hydrophone depths allowed a consistency check on the propagation loss corrections, to be explained in Sec. II E. For simplicity, the hydrophones were deployed without special suspension gear (e.g., damping plates and elastic sections). The hydrophones and cables were attached to a 1 cm diameter braided rope with a 2.5 kg weight at the bottom (see inset of Fig. 1). The hydrophones were held away from the rope and cables with a u-shaped wire stiffener. It was assumed that this would be acceptable for the relatively calm conditions expected in these trials.

Detailed acoustic calibrations of the eight BURB hydrophones were conducted after the trials. The calibration technique involved broadcasting a series of cw tones of known source level at frequencies from 500 to 20 000 Hz in steps of 100 Hz, and comparing results to a reference hydrophone. The measured low-frequency hydrophone responses were near −185 dB re 1 V/μPa. Unfortunately, the hydrophones exhibited a strong resonance in the 6–10 kHz region, with multiple smaller resonances above 10 kHz. These resonances greatly complicated attempts at spectral compensation above 6 kHz. In all that follows, the acoustic data were numerically low-pass filtered with a corner frequency of 5500 Hz. While unfortunate, this reduced bandwidth covered the dominant portion of the ship's signature and was sufficient to explore the effects of directionality and maneuvers on ship source spectra.

Instrumental and background noise levels imposed some constraints on the ship signature measurements. Internal electronic noise levels had an equivalent sound pressure level (SPL) near 50 dB (re 1 μPa^2/Hz), which was more than 40 dB below the typical ship signatures encountered during the trials. More importantly, measured background

acoustic noise SPL were between 60 and 70 dB, decreasing with frequency. An approximate fit to the background noise during the sea trials was found to be $\mathrm{SPL}=118-16\log_{10}(f)$ (dB re 1 $\mu\mathrm{Pa}^2/\mathrm{Hz}$), or approximately equivalent to open-ocean wind-wave noise at Beaufort scale five (wind speeds of 8.5–11 m s^{-1}, as cited in Wenz[7]). Even taking into consideration the shallow-water conditions, which are known to exhibit higher ambient noise at a given sea state, this noise level was in excess of that expected from the local winds (5–6 m s^{-1}). This suggested the presence of the buoys and/or inadequate isolation of the hydrophones from buoy motions as the source of this background noise. Overall, this posed some limitations for higher frequency (>2 kHz) measurements at ship-buoy ranges greater than a few hundred meters. Because of this background noise, the acoustic data were only used for ship-buoy ranges <300 m and where the measured SPL exceeded the background noise curve by 6 dB. This range limit corresponded to approximately 1.5 water depths. Additionally, although the BURB data bandwidth extended as low as 10 Hz, during these trials it was found that cable vibrations and wind-wave impact against the buoy hull generated excess background noise up to approximately 100 Hz. As a result, signals below 100 Hz were ignored.

B. Source ship

These field measurements utilized a small coastal oceanographic vessel, the CCGS VECTOR. This ship is 39.7 m overall length, with maximum beam of 9.5 m, draft of 3.5 m, and displacement of 560 tons. VECTOR has a maximum speed near 6.1 m s^{-1} (11.8 knots). It has a single, three-bladed, variable pitch, 1.8 m diameter propeller driven by an 825 hp (600 kW) diesel engine. The propeller is located 3 m forward of the transom with its axis at 2.3 m depth. A 1.2 m wide by 2.5 m tall rudder is mounted immediately astern of the propeller. In terms of underwater profile, the ship has a straight keel from the bow to approximately 10 m forward of the stern, changing to an upsloping hull form reaching the water line at the transom. A solid fin skeg extends the keel line aft to the rudder post, partially enclosing the propeller. The hull shape in the middle third of the ship blocks near-horizontal forward paths from the propeller within ±28° of the bow.

For these trials, VECTOR was outfitted with two DGPS recorders, one at the bow and one on the aft deck. The aft DGPS was located 4.5 m ahead of the propeller location. The ship's position, speed, and heading over ground were recorded on each system at 1 s intervals. The use of two separate DGPS receivers allowed estimation of the instantaneous ship heading through incoherent differencing of the antenna locations. This technique was used to avoid the complication of tapping into the ship's gyrocompass.

C. Experimental location

These field trials were conducted in Saanich Inlet, near Victoria, BC (Canada). This inlet is approximately 30 km long by 5–8 km at its widest, with depths in the central inlet reaching up to 220 m, overlying a soft sandy mud bottom. For these short-range (<300 m) measurements, seabed reflections were near normal incidence, thus suffering an estimated seabed reflection loss of at least 10 dB at frequencies under consideration here (100 Hz–5 kHz). This reflection loss, in combination with the greater path length (400–500 m), suggests that seabed reflections would be roughly 15–30 dB lower than the direct paths, depending on range. Thus, seabed reflections can be ignored. The inlet is also completely sheltered against ocean swell and has only modest tidal currents. This location is only a few kilometers from the Institute of Ocean Sciences, which provided shore facilities and access to small boats. In April 2005, the surface waters of the inlet were relatively unstratified, with only a mild (0.03 s^{-1}) upward-refracting sound-speed gradient in the upper 90 m. Acoustic propagation modeling suggested that the dominant propagation effects were due to the spherical spreading and surface reflections, and that refraction effects would only be relevant at ranges beyond 1 km. During the trials, the local winds (monitored via a nearby meteorological buoy) were typically 5–6 m s^{-1}, with local wind-wave heights <0.5 m.

D. Signal processing

The fundamental measurement provided by the buoys was the SPL, converted to a frequency spectral density (dB re 1 $\mu\mathrm{Pa}^2/\mathrm{Hz}$) using the individual hydrophone calibrations and the AGC. The goal of this analysis was to determine the vessel spectral source level (SSL, dB) corrected to a standard distance of 1 m. Variations in this SSL with aspect angle, ship speed, and turning rate were investigated, thus requiring estimates at relatively short time intervals. Generally, the measured SPL was strongly dependent on the distance between the source vessel and the buoy. At these short distances, the transmission loss can be approximated by a spherical spreading law and a frequency-dependent absorption term, i.e.,

$$\mathrm{SPL}(f) = \mathrm{SSL}(f) - 20\log_{10}[r] - \alpha(f)r \ (\mathrm{dB\ re\ 1}\ \mu\mathrm{Pa}^2/\mathrm{Hz}), \quad (1)$$

where r is the slant range (m) between vessel and hydrophone and f is the frequency (Hz). The absorption term, $\alpha(f)$, is dependent on water properties (e.g., temperature and salinity)[8] and is generally small ($<3\times10^{-4}$ dB m^{-1}) at frequencies below 5 kHz. It should be noted that reflections from the ocean surface have the potential to complicate the transmission loss calculation (to be discussed in the next section).

The fundamental analysis technique was the calculation of frequency spectra at 1 s intervals. A decision was made to sacrifice frequency resolution in favor of stable, short-duration spectral estimates. The precise measurement of narrowband machinery signals was not a goal in this work. Each BURB channel was processed using 4096-pt fast Fourier transforms, demeaned and tapered using a Hanning window, yielding a 9.8 Hz frequency resolution. For each 1 s block of data (40 000 samples), a total of 17 50% overlapped raw spectra were averaged. In addition to this basic spectral analysis, the data were further averaged within *one-third oc-*

tave bands. A set of industry-standard center frequencies one-tenth decade apart were used, defined by

$$f_c = 10^{n/10}, \quad n = 1,2,3, \ldots \ . \tag{2}$$

For this analysis only six representative bands were used, with corresponding center frequencies of 160, 250, 500, 1000, 2000, and 4000 Hz. Each band was one-third octave wide, with upper and lower frequency limits bounded by multipliers of $2\hat{}(-1/6)$ and $2\hat{}(1/6)$, or 0.8909 and 1.1225 times the center frequency. Averaging into one-third octave bands had the benefits of reducing spectral variability and removing effects of narrowband lines. Spectral averaging was always done using the linear (not decibel) values.

The experimental geometry was well resolved, with estimates of ship-to-buoy horizontal range and ship speed, heading, and turn rate produced at 1 s intervals. The slant range to each hydrophone depth was then used to convert each 1 s averaged SPL to an equivalent SSL using Eq. (1). The typical measurement ranges were between 20 and 300 m. A detailed investigation of the SPL time series found that the maximum acoustic output was coincident with the closest point of approach (CPA) of the propeller. A small geometric correction was applied to the aft-DGPS position to translate the effective center of the ship to the propeller location. The ship turn rate was calculated by differentiation (with smoothing) of the ship heading versus time. An additional calculation was the source azimuthal aspect angle to each buoy. This angle was defined as zero at the bow, 90° at broadside (abeam), and 180° at stern aspect, with an assumption of port-starboard symmetry.

E. Lloyd's mirror effects

It is well known that acoustic interference effects can be created by the combination of direct and surface-reflected acoustic paths. This interference pattern, seen as a range-dependent pattern of alternating peaks and nulls in frequency-time spectrograms, is known as the *Lloyd's mirror* (LM) effect. Important features of this effect are that reflections from the ocean surface can incur only small losses and that the reflection incurs a 180° phase shift. Owing to this reflection, phase shift destructive interference is particularly important at longer ranges and LF, where the difference between direct and surface-reflected path lengths becomes small. In the limit of low-frequency or long range, the source with its surface reflection behaves as a vertically oriented dipole (see Ref. 1, Chap. 4). A LM effect is also possible for seabed reflections, modified by the fact that seabed reflections do not have a 180° phase shift.

A relatively simple theory can be used to quantify the LM effect.[9] The basic theory assumes a point source and receiver, at depths d_0 and d_1, respectively, and specular reflection from a nominally flat ocean surface. The surface-reflected path is assumed to emanate from a virtual source located a distance d_0 above the boundary. The theory also allows use of a reflection coefficient, η, which is less than 1.0 if the boundary reflection is imperfect (this is also useful in the case of seabed reflections). Using these parameters, Lloyd's mirror interference pattern (LMIP) relative to spherical spreading can be given by

$$\mathrm{LMIP} = 10 \log_{10}[1 + \eta^2 - 2\eta \cos(4\pi d_0 d_1 f/(cr))] \quad (\text{in dB}), \tag{3}$$

where c is the (average) sound speed (m s^{-1}) and r is slant range (m). This relation will exhibit a series of peaks and nulls in frequency and/or range, with amplitude controlled by η. Note that this reflection coefficient can differ from unity due to the rough surface scattering and bubble scattering and absorption losses, and thus should generally be regarded as frequency, sea-state, and grazing-angle dependent. For illustration purposes in this discussion, η will be assumed to be 0.8. This theory[9] can also account for refraction effects, which are ignored in this work. This relation predicts frequencies of the first two LM peaks at

$$f_{p1} = cr/(4d_0 d_1) \quad \text{and} \quad f_{p2} = 3f_{p1}. \tag{4}$$

For example, at a slant range of 30 m with $d_0 = 2$ m and $d_1 = 15$ m, the first two peaks are at 375 and 1175 Hz.

Note that the determination of the effective source depth for a ship is not straightforward, as in reality a ship is a complicated, distributed acoustic source. It is generally accepted that the propeller is the dominant acoustic source at lower frequencies.[5] This was confirmed for the VECTOR with the finding that maximum acoustic output coincided with the propeller CPA. However, unless special mountings are used, additional machinery noise can be coupled into the hull and radiate from regions not colocated with the propeller. Additionally, broadband acoustic contributions from breaking bow, quarter, and stern waves and turbulent hull flow will be distributed over the length and depth of the ship hull. Finally, blockage by the hull and absorption by wake bubbles will modify the far-field acoustic output near the bow and stern aspects. Overall, the question can be reduced to consideration of an *effective* source location, spatial distribution, and beam pattern which includes all these effects. Gray and Greeley[5] suggested that an effective source depth for a propeller could be taken as the ship draft minus 85% of the propeller diameter. This is based on the assumption that a given propeller would only cavitate over the top portion of its travel. For the case of VECTOR, this would correspond to a source depth of 2.0 m, which is considerably shallower than ships studied in the references. A modification was proposed by Wales and Heitmeyer,[4] where a vertically distributed acoustic source following a Gaussian distribution in depth was assumed. The corresponding LMIP was then

$$\mathrm{LMIP}_G = 10 \log_{10}\left[\int_0^D (1 + \eta^2 - 2\eta \cos(4\pi d d_1 f/(cr)))W(d)\,\delta d\right], \tag{5}$$

where

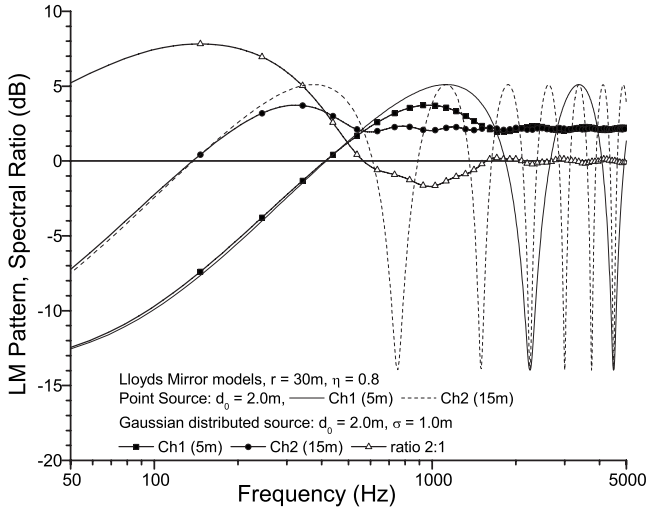

FIG. 2. Predicted LIMP. Example is calculated using point source (d_0 =2.0 m) and Gaussian distributed source (d_0=2.0 m, σ=1.0 m) models with r=30 m and η=0.8. The solid and dashed lines are for point source model with d_1=5 and 15 m, respectively. The solid square and circles denote Gaussian distributed model, with spectral ratio (2:1) denoted by open triangles.

$$W(d) = (\sigma\sqrt{2\pi})^{-1} \exp[-(d-d_0)^2/(2\sigma)]. \quad (6)$$

σ is the Gaussian source standard deviation (m), and D is the ship draft (3.5 m). A normalization constant, which is the integral of Eq. (6) from 0 to D, must be applied. Wales and Heitmeyer[4] found that this provided a better match to the observed LM pattern than using a single (point) source depth. For these trials with the VECTOR, where the ship was operated near top speed during the majority of runs, a significant fraction of the 1.8 m diameter propeller was assumed to be a cavitating acoustic source. Thus, as a starting point, a vertically distributed source with mean depth of 2.0 m and a standard deviation of 1.0 m was assumed in Eqs. (5) and (6). In principle, the source could also be distributed longitudinally, for example, by cavitation bubbles shed by the propeller or rudder. A consequence of such longitudinal source extension would be an increasing directionality at higher frequencies.

A comparison of the predicted LMIP using the two source models is plotted in Fig. 2 as a function of frequency for the two hydrophone depths (d_1=5 and 15 m). A slant range of 30 m (a typical CPA in these trials) and a constant sea-surface reflection coefficient of 0.8 were assumed for this example. The point source model shows the expected alternating peaks and nulls continuing with constant amplitude to frequencies of 5 kHz and beyond. The prediction for the deeper hydrophone shows the pattern shifted to lower frequencies. The Gaussian source case shows similar behavior at frequencies up to the first peak, followed by an increasing attenuation of the higher frequency peaks and nulls. For the Gaussian source case, the frequencies of the first peaks (908 and 303 Hz at 5 and 15 m, respectively) are slightly lower than predicted by Eq. (4), and the peak LMIP was approximately 75% of the point source model peak levels. At frequencies well above the first peak, the distributed source model trends toward a constant LMIP of 2.1 dB for both hydrophone depths. This in agreement with the theoretical asymptote of $10\log_{10}[1+\eta^2]$. At frequencies below the first peak (both point and distributed source models), the LMIP decreases monotonically at approximately 5 dB/octave. In this low-frequency limit, the effective transmission loss approaches twice that due to spherical spreading. It can be shown that for well-behaved source distributions (i.e., symmetric about d_0 and diminishing to zero for large $|d-d_0|$), the first peak in LMIP will always be present, at a frequency very similar to the point source case. The behavior between the first peak and high-frequency limit depends on the specific source distribution. Finally, note that this pattern should scale directly proportional to ship-to-buoy range, such that at ranges >200 m the peaks should be pushed to frequencies greater than a few kilohertz, making the low-frequency roll highly important.

An advantage of measuring the ship signature at two different depths is that the spectral ratio in SSL (uncorrected for LM effect) between the two hydrophones can be used to isolate the frequency dependence of the LM effect independent of the shape of the ship source spectrum, i.e., that $\mathrm{SSL}_{15\ \mathrm{m}}-\mathrm{SSL}_{5\ \mathrm{m}}=\mathrm{LMIP}_{15\ \mathrm{m}}-\mathrm{LMIP}_{5\ \mathrm{m}}$. With a single hydrophone, the LM effects are not easily separable from structures in the ship SSL. Specifically, the distributed source depth, standard deviation, and the frequency dependence in η are free parameters which can estimated through fitting Eqs. (5) and (6) to this ratio. The predicted ratio in LMIP between the two channels is plotted in Fig. 2. The distributed source model prediction is that the ratio will be up to +7 dB below 400 Hz, dipping to a −2 dB null near 1000 Hz, and finally trending to +0 dB at frequencies above approximately 1500 Hz. For the same source depth, the point source model would yield a recurring series of strong peaks and nulls extending to high frequencies. This sensitivity to source depth distribution illustrates the potential use of this spectral ratio technique in estimating the effective source distribution. This will be examined using sea-trial data in the next section.

III. ACOUSTIC MEASUREMENTS

A goal of this analysis is to quantitatively determine SSL dependencies on frequency, speed, aspect angle, and turn rate. The intended outcome is a simple empirical model that can be used to predict ship signature during maneuvers. In this work, it was assumed that the variation in SSL can be decomposed into independent variations with ship speed (U, m s^{-1}), aspect angle (θ, deg), and turn rate (TR, deg/s), i.e., as

$$\mathrm{SSL}(f,\theta,U,\mathrm{TR}) = \mathrm{SSL}_B(f) + S_U(U) + S_{\mathrm{AA}}(\theta) + S_{\mathrm{TR}}(\mathrm{TR}) \quad (\text{in dB}), \quad (7)$$

where SSL_B is the broadside SSL at a reference speed, and S_U, S_{AA}, and S_{TR} are the normalized variations due to speed, aspect angle, and turn rate, respectively. The broadside SSL and variations due to speed and aspect angle will be extracted from the straight, constant-speed runs. Analysis of the turning maneuvers will attempt to isolate the variation due to turn rate. Note that Eq. (7) might also include contributions from ship acceleration. However, no specific tests were con-

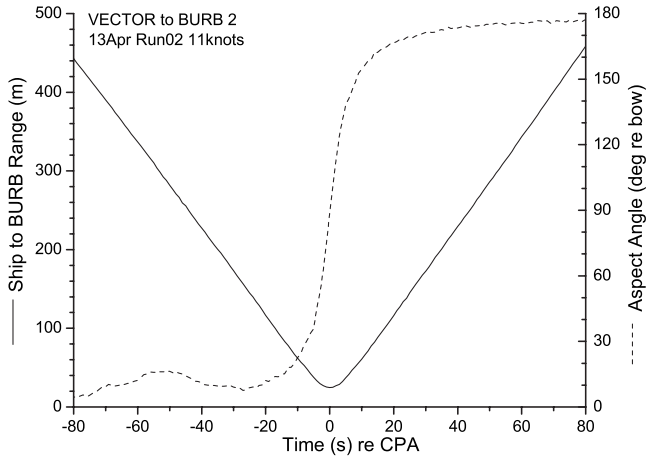

FIG. 3. Variation in ship-to-BURB range and aspect angle during a straight-line run at 5.7 m s^{-1} (11.0 knots). CPA was 24.8 m.

ducted in this trial to measure this effect, so it will be ignored herein.

A. Examination of Lloyd's mirror effects

Prior to examining specific results, it was important to understand and possibly compensate for the LM effects. An example typical of the straight, constant-speed runs will be examined in detail. In these runs, the four buoys were placed in a line and the ship directed to steam at a constant speed along a parallel course approximately 30–50 m away from the line of buoys. Figure 3 shows an example of the variation in ship-buoy geometry as the VECTOR conducted a straight, constant-speed run at 11.0 knots (5.7 m s^{-1}). In this example, the ship passed through a CPA of 28.4 m and was within 300 m of the buoy for a period of about 106 s. As it transited past the buoy, the ship exhibited a hyperbolic range-time trajectory, i.e.,

$$r^2 = r_0^2 + (U(t - t_0))^2, \tag{8}$$

where r_0 and t_0 are the range (m) and time (s) of CPA. The aspect angle varied smoothly from approximately 5° to 175° during the transit, with a rapid transition through broadside aspect within ±10 s of CPA. In this geometry, the sea-surface grazing angles were relatively small, increasing from approximately 1.3° at 300 m range (shallow hydrophone) to a maximum of 30° (deeper hydrophone) at the 30 m CPA.

Figure 4 shows the SSL spectrograms from the two channels on one of the BURBs during this straight, constant-speed transit. These spectra were corrected as in Eq. (1) but not corrected for the LM effect described in Sec. II E. Lines indicating the expected first LM peak frequencies [Eq. (3)] are overplotted. Both spectrograms show a relatively smooth decrease in radiated signature with increasing frequency, with several clusters of narrow-band lines (300–800, 1100–1600, and near 2320 Hz) due to ship's machinery. Although there was a clear SSL maximum at CPA, suggesting a broadside directional peak, a clear LM pattern was not observed. If LM effects were present, the SSL spectra in both channels should exhibit a hyperbolic shaped peak feature (similar to the dashed lines), centered at CPA, with a strong decrease in SSL below the first peak. This low-frequency roll-off should be particularly obvious at times >±10 s from CPA, corresponding to ranges >100 m. Also, the shallower hydrophone (channel 1) should show a stronger low-frequency decrease than the deeper hydrophone. These features were not observed. This lack of LM structure is believed to be due to the

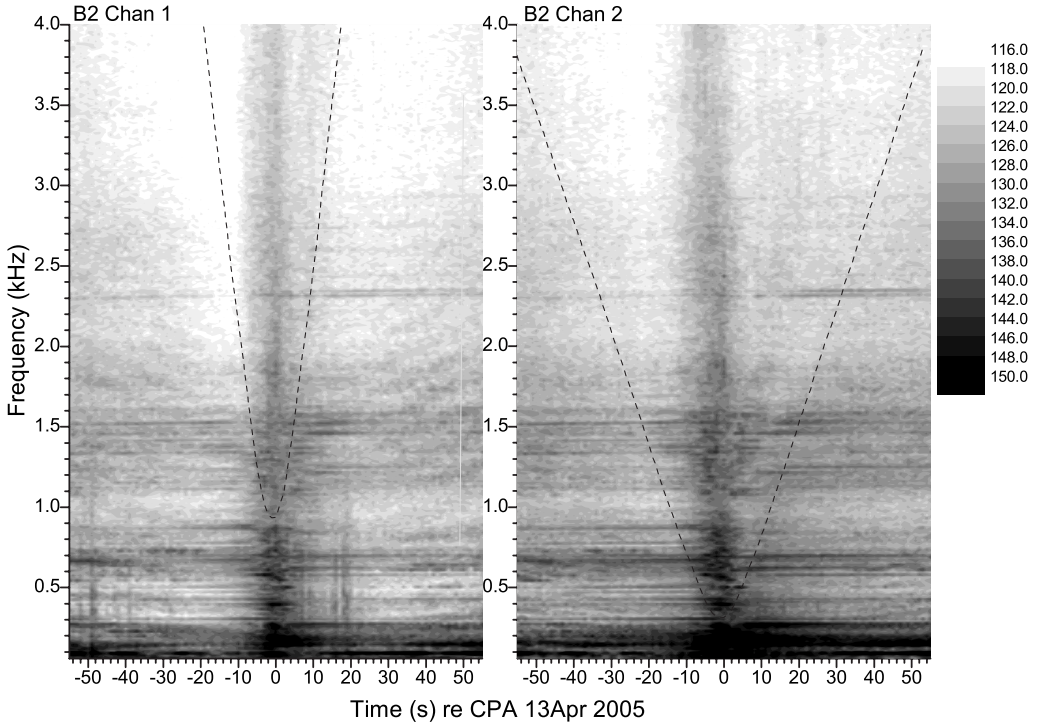

FIG. 4. Example frequency-time SSL spectrograms for the two channels (left 5 m depth, right 15 m depth) of a BURB during a straight, constant-speed run at 5.7 m s^{-1} (11 knots). Intensity in dB re 1 $\mu Pa^2/Hz$ at 1 m. Spectra have not been corrected for LM propagation effects. Frequencies of the first LM peak [Eq. (4)] in each channel are overplotted.

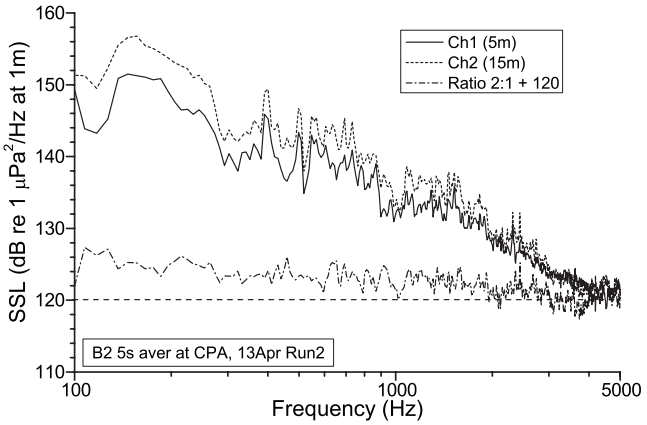

FIG. 5. Example SSL spectra at two depths near CPA from one BURB during a straight, constant-speed run at 5.7 m s^{-1} (11 knots). Spectra are averaged over 5 s, but uncorrected for LM effects. Spectral ratio (Chan 2:1) +120 dB is plotted as dash-dot line.

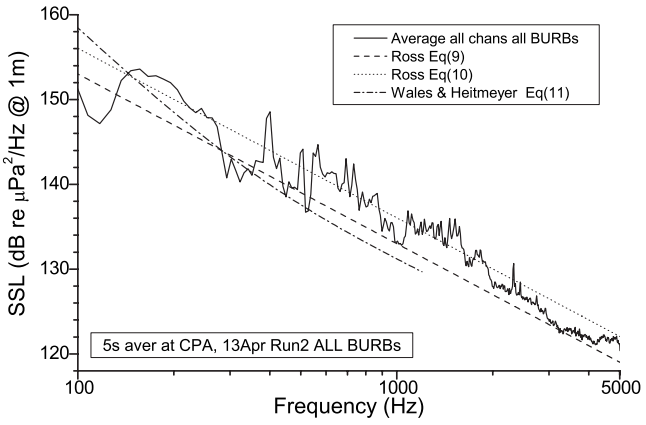

FIG. 6. Comparison of averaged SSL spectrum at broadside incidence from a straight, constant-speed run at 5.7 m s^{-1} with regressions due to Ross (Ref. 1) Eqs. (9) and (10) and Wales and Heitmeyer (Ref. 4) Eq. (11). Measured spectrum was averaged over 5 s at CPA, then averaged over the two channels from all four BURBs.

shallow source depth (~2.0 m) combined with blocking of the surface reflection from the ship's hull at forward aspect and acoustic scattering and absorption by the wake near stern aspect.

A further check for the presence of the LM effect can be made by detailed comparison of the ship's SSL at the two hydrophone depths near CPA (Fig. 5), corresponding to broadside incidence. At CPA, the LM effects should be pronounced due to larger grazing angles and minimal hull blockage. The figure shows a slightly stronger SSL in the deeper hydrophone at frequencies below 2 kHz, with a maximum spectral ratio near +6 dB at 100 Hz, in rough agreement with the prediction. The predicted asymptotic decrease in spectral ratio to near unity above 2 kHz (shown in Fig. 2) is also present; however, the prominent null near 1 kHz is absent. Even if the actual source depth distribution differed from the assumed values, there should still be a frequency-varying spectral ratio and a prominent null in this ratio in the vicinity of 1 kHz. Furthermore, below roughly 500 Hz (particularly in channel 1) the observed uncorrected SSL should be approximately flat, with the 5 dB/octave decrease due to the LMIP canceling out the roughly f^{-2} behavior (6 dB/octave increase) in the true SSL (see Sec. III B) at LF. This was not observed. It is possible that measurements below 200 Hz were contaminated by background noise, particularly in channel 1 which has a lower SSL. In the absence of a clear LM pattern, and without any confirmation of the exact form of the low-frequency LMIP, it would seem imprudent to apply any corrections in this case. Averaging the SSL estimates between hydrophone channels at two depths, and between buoys at different locations, should minimize these LM effects, with the caveat that resulting estimates below 200 Hz may be underestimated by up to approximately 6 dB.

B. Source level estimates and directionality

A series of straight, constant-speed runs was performed to establish a base line SSL for the VECTOR as a function of speed. Additionally, the variation in estimated SSL as the ship transited past the BURB field was used to infer the source directionality. The measured SSL near broadside incidence were in reasonable agreement with empirical reference spectra, as shown in Fig. 6. In this figure, the estimated SSL spectrum was averaged over 5 s at CPA, then over the two hydrophone channels in each buoy, and then over similar CPA at each of the four buoys. The variability in this estimate between the buoys decreased from ±2 dB at 100 Hz to ±1 dB at 500 Hz and above. The reference spectrum due to Ross[1] is

$$\mathrm{SSL}(f) = 190 + 53\log_{10}(U/5.15) - 20\log_{10}(f) \quad (\mathrm{dB\ re\ 1\ }\mu\mathrm{Pa}^2/\mathrm{Hz}), \tag{9}$$

where U is the ship speed (m s^{-1}). Ross also proposed an alternate reference curve based on propeller characteristics,

$$\mathrm{SSL}(f) = 195 + 60\log_{10}(U_t/25) + 10\log_{10}(B/4) - 20\log_{10}(f), \tag{10}$$

where U_t is the propeller tip speed (m s^{-1}) and B is the number of blades. For the VECTOR during this run, the propeller was operated at 290 rpm, equivalent to U_t=27.3 m s^{-1}. A more recent study by Wales and Heitmeyer[4] generated a different relation, without a speed dependence, fit to an ensemble of measurements on roughly 50 merchant ships over a 30–1200 Hz band, i.e.,

$$\mathrm{SSL}(f) = 230 - 35.9\log_{10}(f) + 9.17\log_{10}(1 + (f/340)^2). \tag{11}$$

The typical ship speeds in the Wales and Heitmeyer study were between 10 and 15 knots. All of these empirical references represent averages among an ensemble of different merchant and naval ships, with typical variability of ±6 dB about the mean, thus the signature of particular ship may not be an exact match. Overall, there is a reasonable agreement in level and frequency dependence between the measured and reference spectra at frequencies above 150 Hz. This suggests that VECTOR can be considered a *typical* ship from an acoustic signature perspective, in spite of its relatively small size. The VECTOR signature contained a number of narrowband machinery lines approximately 2–5 dB higher than the

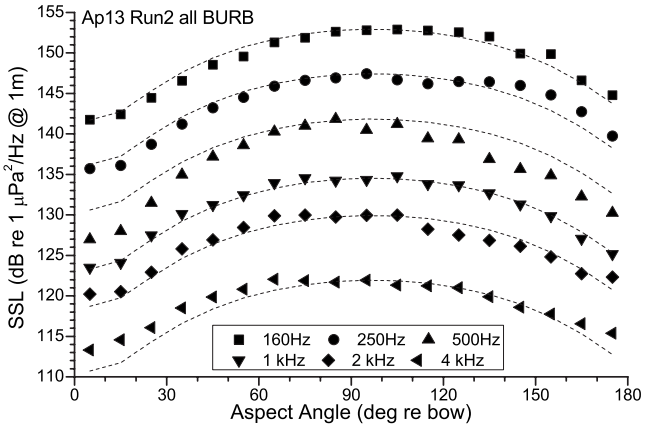

FIG. 7. Variation in one-third octave averaged SSL at six frequencies vs aspect angle from a straight, constant-speed run at 5.7 m s^{-1} (11 knots). SSL was averaged within 10° bins over the two channels from all four BURBs. The dashed lines are Eq. (12) scaled to match broadside aspect values at each frequency.

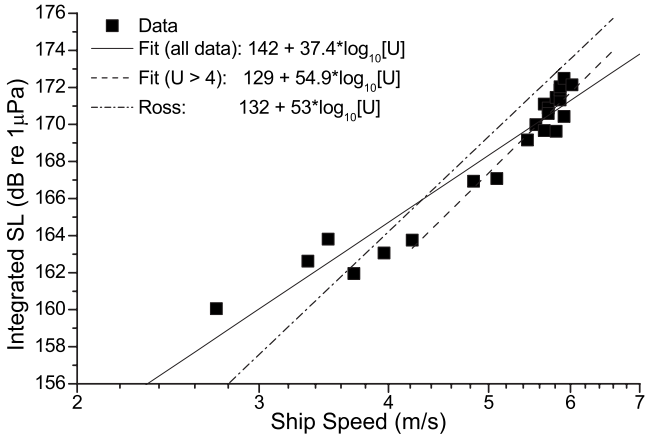

FIG. 8. Variation in BSL (dB re 1 μPa) vs speed (m s^{-1}) from all straight, constant-speed runs conducted on April 12 and 13, 2005. Source levels were calculated from 5 s averaged SSL taken at CPA (broadside aspect) to each of three buoys. The solid line is the least-squares linear regression to the entire data set. The dashed line is fit to data where speed >4 m s^{-1}. The dash-dot line is the equivalent speed dependence from Ross (Ref. 1).

references. There were particularly prominent lines at 400, 500, 550–870, 1060–1570, and 2320 Hz. Either this measured SSL, or a fit of the data to $\log_{10}(f)$, can be utilized as an estimate of $\mathrm{SSL}_B(f)$ in Eq. (7).

By averaging the SSL spectra over the two hydrophones on each BURB and then into one-third octave frequency bins, stable estimates of the source directionality were produced (Fig. 7). This plot was generated by averaging within 10° angular bins all available SSL versus aspect angle estimates, taken at 1 s intervals, from all four BURBs. Averaging within 10° angular bins compensated for the large number of estimates near bow and stern aspects, but only a few near broadside aspect. The figure shows that VECTOR exhibited a clear broadside peak approximately 8–12 dB higher than at bow incidence. This directionality appeared to be marginally stronger at lower frequencies. There was also a clear bow-stern asymmetry, particularly at lower frequencies, with the stern aspect approximately 2–4 dB higher than at bow aspect. There was only a small variation in SSL within 20° of the bow across all frequencies. This bow-stern asymmetry was presumed to be due to acoustic blocking by the hull in the forward direction.

A simple, frequency-independent model for this aspect angle variation was created. This was performed by normalizing the variation at each frequency and then averaging the resultant directionality patterns across frequencies. The resulting normalized variation with aspect angle, denoted S_{AA}, was found to be in close agreement with

$$S_{\mathrm{AA}} = 10\log_{10}[\cos^{1.95}(\theta - \theta_0) + 0.08] \quad (\mathrm{dB}), \tag{12}$$

where $\theta_0 = 97°$ is the peak direction. The small constant offset was added to handle small values near bow aspect. This curve, suitably denormalized to match the broadside aspect SSL, is plotted in Fig. 7, and will be used to correct for aspect angle effects in subsequent sections. The data-model comparison highlights the slightly greater directivity at the three lower frequencies. This angular variation is close to the expected angular variation for a horizontally oriented dipole (i.e., cosine squared), with the main lobe axis oriented 7° aft of beam (and assumed symmetric port-starboard). The data do not show any significant increase in directivity with frequency, as might be expected from a horizontally distributed source.

C. Speed dependence

A total of 12 straight runs at nominal speeds from 2.6 to 6.2 m s^{-1} were conducted during the first two days of operations, allowing examination of the speed dependence in SSL. Here, we were interested only in the variation in broadband source level (BSL) with speed, integrated from 120 Hz to 5 kHz. This was computed from 5 s averaged SSL at CPA from each buoy. In practice, there were always small variations in speed, roughly ± 0.25 m s^{-1}, during each run as the ship attempted to maintain the requested speed while lining up the buoys for a 30–50 m CPA. Using the measured speed at CPA to each buoy, a number of independent BSL versus speed estimates were created from each run (see Fig. 8). Although there was some scatter in the measurements, there is a clear trend of increasing BSL versus speed. A linear regression to these data yielded the relation

$$\mathrm{BSL} = 142.0 + 37.4\log_{10}(U). \tag{13}$$

The regression generated a correlation coefficient of 0.97 from a total of 22 data points. Note that this results suggests a speed dependence significantly weaker than the $U^{5.3}$ specified by Ross [in Eq. (9)]. A possible explanation for this difference is that these measurements spanned a lower range of speeds compared to Ross' regressions, which were based on speeds from 8 to 24 knots (4.1–12 m s^{-1}). At the lower speeds, the acoustic signature of the VECTOR likely included increasing contributions from nonpropulsion related machinery (e.g., generators and ventilation). If we restrict attention to BSL estimates at speeds greater than 4.0 m s^{-1}, the best fit line has slope of 54.9 (see Fig. 8), which is in agreement with Ross' result. When compensating for speed variations between 4 and 6 m s^{-1} during turning maneuvers (described below), this latter speed dependence seems appropriate.

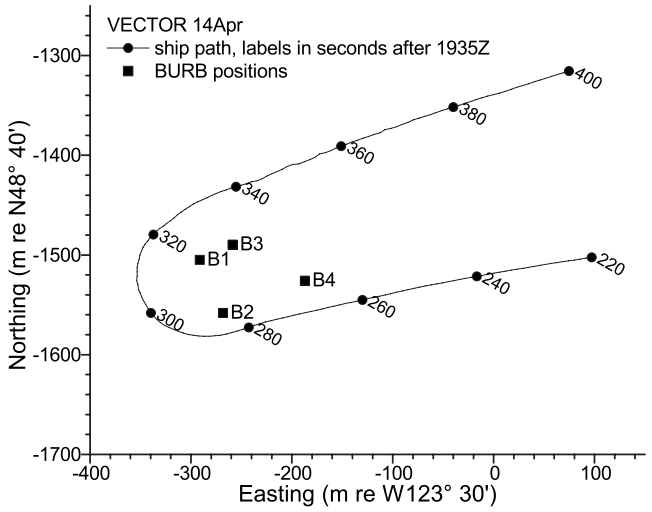

FIG. 9. Plan view of trajectory of CCGS Vector relative to the four BURBs during a 180° turning maneuver on April 14, 2005. Inbound ship speed was 5.8 m s^{-1} (11.2 knots). Labels are time (s) after start of run at 1935Z.

D. Turning maneuvers

During the turning maneuvers, the VECTOR exhibited significant increases in acoustic signature relative to the straight runs. This was true of both 90° and 180° turns. An important feature of these maneuvers was a simultaneous variation in ship speed and turning rate through the evolution of the turn. This reduction in speed was a consequence of the turning maneuver and not a result of a deliberate reduction in engine power or rpm. An additional complication was that, because the buoys occupied slightly different locations, they each were presented with different aspect angles during the turn. Figure 9 shows a plot of the ship track relative to the buoys through a 180° turning maneuver, and Fig. 10 shows the corresponding speed and turning rate. In this maneuver, the inbound speed was 5.8 m s^{-1} (11.2 knots), executing a 180° turn to starboard of radius 68 m in roughly 55 s. In this example, the turn was initiated at 275 s. After a brief transition, there was a period of relatively constant turn rate, near 4 deg/s, between 295 and 315 s. Note that there were two significant events in this maneuver: (1) the turn initiation extending over the first 15 s, and (2) a point of minimum

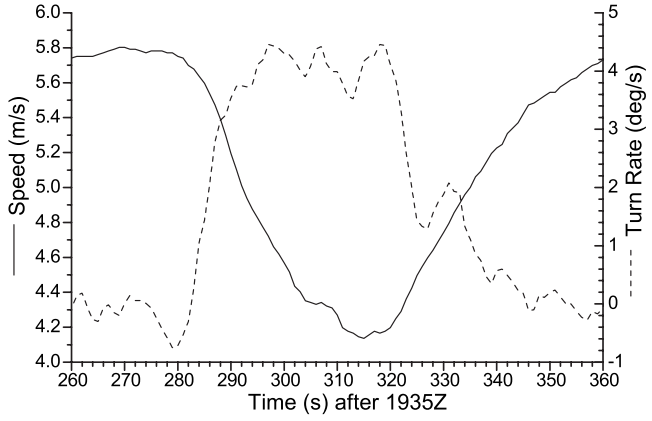

FIG. 10. Variation in ship speed (m s^{-1}) and turn rate (deg/s) during a 180° turning maneuver on April 14, 2005 (as shown in Fig. 9).

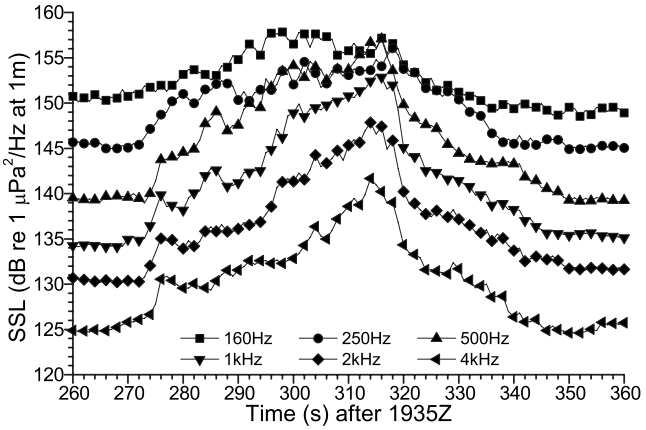

FIG. 11. Time series of corrected one-third octave averaged SSL at six frequencies from the same 180° turning maneuver, as shown in Figs. 9 and 10. SSL data have been corrected for aspect angle and speed dependence as described in the text, then averaged among three buoys.

speed, approximately 50 s into the turn. These events have acoustic significance (discussed below). Through the course of the turn, the ship presented nearly the full range of aspect angles to the individual BURBs.

The first step in this analysis was to correct for the simple variations due to speed and aspect angle [Eqs. (12) and (13)], applied to the one-third octave averaged SSL values. Since the speed was always above 4 m s^{-1}, the speed correction was taken as $S_U = 54.9 \log_{10}[U/U_0]$, where U_0 is the inbound speed. After the aspect angle and speed correction, the time series of one-third octave SSL estimated from the individual BURB data were quite similar, and so were averaged together. Figure 11 shows the corrected one-third octave averaged time series, equivalent to $SSL_B + S_{TR}$ at a speed of 5.8 m s^{-1}, through this turning maneuver. At the initiation of the turn (275 s), there was a relatively rapid rise in SSL of between 4 and 10 dB, particularly at the higher frequencies, as the ship sets its rudder and began to heel into the turn. At this point, the ship was still near its in-run speed. After the turn initiation, the behavior at lower (160 and 250 Hz) and higher frequencies began to diverge. At LF, the corrected SSL exhibited a broad plateau up to 8 dB above the in-run condition, dropping away only after the minimum speed point (315 s). The higher frequencies exhibited a slow ramp-up during the turn ending in a pronounced peak coincident with the minimum speed point. For example, at 4 kHz the SSL rose from a base line near 125 dB to a peak of 141 dB. At the minimum speed point, the ship speed was 4.2 m s^{-1} (8.1 knots), or 72% of its inbound speed. At this point, the commanded propeller rpm (still set for 5.8 s^{-1}) was furthest from constant-speed equilibrium. This can be seen through changes in the propeller advance ratio,

$$J = U/(nD_p), \tag{14}$$

where n is the propeller rotational speed (rev/s^{-1}) and D_p is the propeller diameter (1.8 m). At the in-run speed of 5.8 m s^{-1}, the propeller was at 285 rpm, thus operating at $J = 0.674$. At the minimum speed point, the advance ratio was reduced to 0.488. In general, as J decreases, the propeller thrust and torque increase and the propulsive efficiency de-

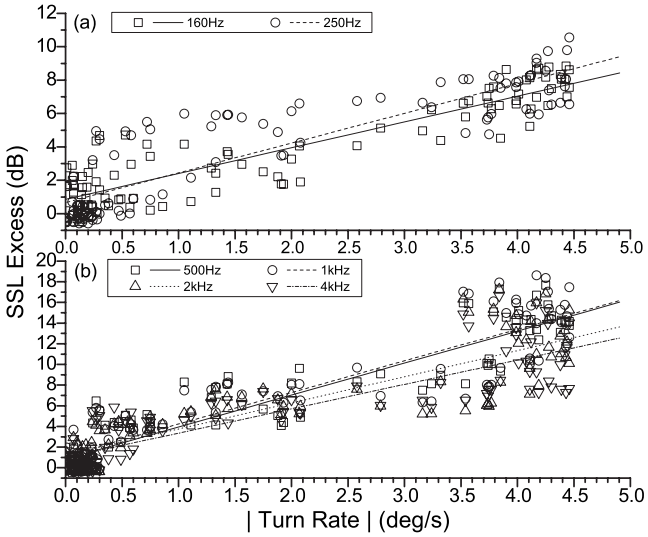

FIG. 12. Variation of SSLE with ship turn rate, from the same 180° turn maneuver shown in Figs. 9–11. (a) One-third octave variations at 160 and 250 Hz. (b) One-third octave variations at 0.5, 1.0, 2.0, and 4.0 kHz. Lines are least-squares linear regressions to data.

creases (see Ref. 1 Sec. 8.3). Increasing the propeller thrust and torque presumably created the observed increase in radiated signature levels. It is also possible that strong application of the rudder contributed to the initial signature peak (near 276 s).

The dependence of SSL excess (SSLE=S_{TR}) on turn rate was complicated. Figure 12 shows the variation of SSLE with turn rate explicitly, calculated from data shown in Fig. 11 through normalizing by SSL_B calculated from the in-run. The figure separates the dependency at the two lowest frequencies (160 and 250 Hz) from the higher frequency behavior. Figure 12(a) shows an approximately linear dependence of SSLE on turn rate, with slopes near 1.65. The maximum low-frequency SSLE was near 10 dB. In particular, for the relatively constant turn rate portion (TR$>$3 deg/s), the variance was small. However, at 500 Hz and above [Fig. 12(b)], the dependence on turn rate was more complicated. The best fit lines have higher slopes (3.1, 3.1, 2.5, and 2.4 at 500 Hz, 1 kHz, 2 kHz, and 4 kHz, respectively), with significantly greater variance at higher turn rates. In particular, there appeared to be a region of higher SSLE, up to 18 dB at turn rates above 3.5 deg/s, which was not present at the lower frequencies. These higher SSLE values occurred near the minimum speed point, which is suggestive that there may be an additional dependence on the propeller advance ratio. There were also some anomalously low SSLE values at TR $>$3 deg/s in the 4 kHz data, which occurred early in the turn.

IV. SUMMARY AND RECOMMENDATIONS

A. Summary discussions

This work describes an investigation of surface ship underwater acoustic signatures with particular examination of directionality and the effects of maneuvers. The prototype instrumentation, while suffering from some practical limitations, successfully delivered broadband acoustic measurement with a well-resolved experimental geometry. Overall, this supported the establishment of empirical models for the aspect angle, speed, and turning rate variations. The use of self-contained buoys was successful from a ship-handling perspective, allowing the ship to freely maneuver close to the buoys in relatively deep water. The target ship could quickly deploy and recover these buoys, making this approach convenient for self-ranging.

Broadband measurements from approximately 150 Hz to 5 kHz were demonstrated herein. The lower bound was set by LF noise contamination due to wave impacts against the buoy hull and inadequate hydrophone suspension. The upper frequency limit was imposed by hydrophone response problems. Both of these limitations can be overcome. Improvements in LF performance can be made by deploying the hydrophones at greater depths below the surface buoys (e.g., $>$20 m) and adding a compliant, damped suspension similar to that utilized by sonobuoys. The greater receiver depth also pushes the LM patterns to lower frequencies (at a given range), allowing measurement at greater ranges. A redesign of the buoys themselves, minimizing the surface-piercing components, would reduce LF noise due to waves. High-frequency performance can be improved through the use of better quality hydrophones.

An examination was made of the potential effects of LM interference patterns, with the conclusion that *for this particular ship* there was no convincing evidence for these effects. A technique to account for the LM propagation effect was presented, including use of a vertically distributed source model and examination of the spectral ratio between two receiver depths. In the present measurements with the VECTOR, the expected LM pattern of peaks and nulls in frequency-time spectrograms was absent. Use of a vertically distributed source model can explain the lack of higher-order interference peaks and nulls; however, the first peak should be present. Furthermore, at frequencies below the first peak the predicted strong roll-off in uncorrected SSL estimates, expected to be particularly prominent in the shallow hydrophone at ranges beyond 100 m, was not observed. The reason for this lack of LM structure was believed to be blockage of the surface reflected path due to shadowing by the ships hull near bow aspect and acoustic absorption by the wake near stern aspect. This absence of a LM interference pattern should not be taken as universal, as it has been seen in other cases (e.g., Wales and Heitmeyer[4]) with larger vessels. The final approach taken was to not apply any LM corrections, and simply average SSL estimates between receiver depths and from buoys at different locations. The caveat in this approach being that SSL estimates below approximately 200 Hz may be underestimated by up to 6 dB.

In straight-line, constant-speed runs, the ship acoustic signature at broadside incidence was found to agree closely with well-established empirical relations. Specifically, above 150 Hz, the SSL estimates exhibited close to an inverse-frequency-squared dependence, in general agreement with models proposed by Ross[1] and Wales and Heitmeyer.[4] An examination of the broadband SL versus ship speed, over the range of 2.6–6.2 m s^{-1}, showed a dependence approximately as speed to the power of 3.8. This is significantly lower than

the 5.3 power dependence proposed by Ross, which was generated for an ensemble of much larger ships over a greater range of speeds ($4-12$ m s^{-1}). However, these present measurements included lower speed measurements than the Ross relations, which presumably included acoustic contributions from nonpropulsion machinery such as generators. A regression of broadband SL versus ship speed for data above 4 m s^{-1} was in complete agreement with the Ross result. In this context, a measurement of the ship SSL while stationary would be a useful supplement.

The VECTOR signature exhibited significant horizontal directionality. Relative to the broadside maximum, the bow aspect SSLs were reduced by 10–12 dB depending on frequency. Averaged over frequency, the aspect angle dependence was in approximate agreement with a cosine-squared model, with the main lobe directed 7° aft of beam (with assumed port-starboard symmetry). The lack of increasing directivity at higher frequencies suggested that there was no along-ship extent to this acoustic source. This directionality is hypothesized as due to a combination of true source (propeller) directionality, shadowing by the ship hull, and wake absorption effects. Arveson and Vendittis[3] showed similar directionality in near-horizontal aspect angle measurements on a larger cargo ship. Specifically, their measurements showed a 16 dB variation between bow and beam aspects at 350 Hz, with a roughly 6 dB bow-stern asymmetry. However, their measurements also showed more omnidirectional behavior in very LF (<30 Hz) narrowband propeller and machinery tones.

During turning maneuvers, the VECTOR exhibited signatures up to 20 dB above the beam aspect values from straight runs at the same speed. An important feature of these turning maneuvers was a simultaneous variation in aspect angle, speed, and turning rate. By correcting for the previously established variations in aspect angle and speed, a SSLE relative to broadside was estimated. This SSLE was mostly attributable to turn rate variations. At the initiation of the turn, there was a relatively rapid rise in SSLE of between 4 and 10 dB as the ship set its rudder and began to heel into the turn. The maximum SSLE occurred during a second peak, approximately 50 s after the start of the turn, coincident with point of minimum speed. When examined in terms of turn rate dependence, while there was a clear trend of increasing SSLE with TR, the behavior was complicated. At 160 and 250 Hz, there was a simple linear dependence on turn rate with maximum SSLE up to 10 dB. At 500 Hz and above, the SSLE showed additional signature output, up to 18 dB, near the point of minimum speed. This additional signature output was hypothesized as due to the fact that the commanded propeller rmp was set for a speed significantly above the actual ship speed. This is similar to an acceleration transient where the propeller advance ratio would be significantly below optimal. This present data set, in particular, with its lack of specific data on acceleration effects and lack of instantaneous machinery data (e.g., propeller rpm and torque), was deemed insufficient to fully separate variations due to the acceleration and turning rate.

It is unclear as to whether results from the VECTOR would be more generally applicable to large merchant and naval ships. During straight, constant-speed runs, VECTOR exhibited broadside SSL and speed dependencies in agreement with reference curves, generated from ensembles of larger ship signatures. This suggests that its signature was typical of this broader class of ship. Thus, it seems reasonable to expect that straight-course directionality patterns might be similar, as other measurements (for example, Arveson and Vendittis[3]) have shown. However, larger vessels (particularly merchants) would have some difficulty in executing the tight turning maneuvers demonstrated herein, and only the most powerful ships would be able to maintain speed during such turns. Clearly, one should expect detailed differences in SSL between ships of different sizes (particularly draft), different hull forms, different number of propellers and rudders, and greater maximum speed. Deeper draft vessels (5–8 m source depths) have been found to exhibit clear LM propagation effects.[4] Significant differences may be exhibited by twin-propeller ships during turns as the heel of the ship moves the outside propeller deeper and the inside propeller shallower. Also, at higher speeds, the vortex shedding and wake bubble generation effects may spread acoustic sources in the along-ship dimension, which would influence directionality.

The analysis on turn rate dependency implicitly required an assumption that the aspect angle and speed dependencies were similar during turns and straight runs. The turn rate dependence then became a catch-all parameter after the assumed directionality and speed dependence had been removed. Greater exploration of this assumption is recommended through a set of carefully controlled experiments, varying the turn rate through changing the ships turning radius while adding extra throttle to maintain speed. It has been suggested that coupling between speed and turn rate may be such that their variations could be condensed into the ratio U/TR. The present data set do not span sufficient variations in these variables to assess this. Also unassessed by these data was whether there was a difference in radiated acoustic signature between the inside and outside of the turn. For safety reasons during these sea trials, the buoys were always located on the inside of the turn.

B. Recommendations for portable acoustic ranging

This section summarizes practical lessons learned during the sea trials with the VECTOR and similar trials with other ships.

(1) In order to fully quantify the ship signature including maneuvers, the following types of measurements are recommended, with multiple trials of each type as time allows:
   (a) straight, constant-speed runs at a variety of speeds.
   (b) SSL while the ship is drifting (very low speed).
   (c) Straight accelerating runs from low to maximum speed, possibly varying the applied power level.
   (d) 180° or 360° turning maneuvers at variety of fixed speeds and turn rates. In practice this implies maintaining constant speed through variation in throttle and varying the turn rate through specific rudder angles at a given speed.

(2) Ship-to-buoy CPA should be between approximately 50 and 100 m, increasing slightly for higher speed runs. Small CPA have the potential to overload receivers, and (for straight runs) provide only a small number of measurements at aspect angles near broadside.
(3) Buoy placement should attempt to provide both port and starboard aspects in the case of straight runs, and inside versus outside of the turn measurements in the case of maneuvers. This requires careful buoy placement to allow the ship to maneuver safely through the buoys.
(4) A set of at least two buoys should be deployed in order to provide spatial diversity, effective coverage of port-starboard, or inside-outside turn geometries, and measurement redundancy in the event of buoy malfunction. A set of four buoys was found to be reasonably easy to deploy and recover.
(5) Hydrophone depths should be greater than 20–30 m to provide separation from noise created by wave action on the surface float. Larger receiver depths also push the LM interference pattern to lower frequencies and allow measurements at greater horizontal ranges in the case of downward-refracting near-surface sound-speed gradients. The hydrophone cables should be decoupled from motions of the surface buoys through the use of compliant, damped suspension gear.
(6) The buoys should have two independent hydrophones deployed at two different depths. This allows verification of surface-reflected interference effects and potentially allows estimation of the effective source depth distribution and sea-surface reflection coefficient.
(7) Good quality hydrophones with relatively flat frequency response up to at least 20 kHz should be utilized. Integral preamplifiers will ensure sufficient electronic noise immunity through the relatively long cables.
(8) Each buoy should be equipped with a differential GPS receiver, recording positions at 1 s intervals. Similar DGPS recorders should be installed on the source ship. This allows calculation of parameters, such as ship-to-buoy range and aspect angle. Using two DGPS systems on the ship, located at the bow and stern, allows calculation of the instantaneous ship heading. Alternately, recording the ship's gyrocompass output (if feasible) or use of short base line, multiple receiver GPS arrays will provide improved measurement of the ship heading.
(9) The buoys should be designed to minimize the surface-penetrating area, presumably through use of a spar-buoy concept. This would reduce wave impact noise against the buoy hull and reduce vertical excursions of the buoy. The only above-water requirement is for support of the GPS receiver and whatever aids to navigation are required (e.g., radar reflectors). Addition of a remote position relay system would enable the ship to better maneuver around the buoys, and find them quickly during the recovery phase.
(10) During the VECTOR trials, important ship's propulsion information, such as propeller rpm, pitch, torque, and rudder angle, were recorded manually and did not account for rapid changes during turns. It is highly desirable to automatically record ship machinery state during runs. A data recording rate of 1 sample/s is recommended for maneuvering runs.
(11) Measurements should be conducted in a sheltered, relatively deep-water location, preferably in water depths greater than 200 m and over soft, acoustically absorbent seabeds. This minimizes background noise and seabed reflection interference.
(12) In these trials, the various maneuvering runs were conducted quickly, with typically less than 15 min. intervals between successive runs. However, care must be taken to ensure that bubbly wakes from previous runs have had sufficient time to dissipate. This is particularly important for higher speed, aggressive maneuvers where there is strong wake generation. It is recommended that a minimum of 20–30 min be allowed between successive runs.

ACKNOWLEDGMENTS

This work was made possible by the Defence R and D Canada Technology Investment Fund program. CCGS VECTOR ship time was provided by Fisheries and Oceans Canada, with additional laboratory and boat facilities provided by the Institute of Ocean Sciences (Sidney, BC). The authors wish to thank Mr. Ron Teichrob and Nick Hall-Patch of the Institute of Ocean Sciences for their assistance in BURB technical issues, including hydrophone calibrations. The Master, Officers, and crew of the CCGS VECTOR are acknowledged for their expert ship-handling and instrumentation deployment skills during the sea trials in Saanich Inlet. Mr. Richard Johnson of DRDC Atlantic conducted the BURB hydrophone calibrations.

[1]D. Ross, *Mechanics of Underwater Noise* (Peninsula, Los Altos, CA, 1987).
[2]P. Scrimger and R. Heitmeyer, "Acoustic source level measurements for a variety of merchant ships," J. Acoust. Soc. Am. **89**, 691–699 (1991).
[3]P. Arveson and D. Vendittis, "Radiated noise characteristics of a modern cargo ship," J. Acoust. Soc. Am. **107**, 118–129 (2000).
[4]S. Wales and R. Heitmeyer, "An ensemble source spectra merchant ship-radiated noise," J. Acoust. Soc. Am. **111**, 1211–1231 (2002).
[5]L. Gray and D. Greeley, "Source level model for propeller blade rate radiation for the world's merchant fleet," J. Acoust. Soc. Am. **67**, 516–522 (1980).
[6]M. Trevorrow, S. Vagle, and N. Hall-Patch, "Description and field evaluation of the broadband underwater recording buoy system," DRDC Atlantic Report No. TM 2005-231, Defence Research and Development Canada Atlantic, of Dartmouth, Nova Scotia, 2005.
[7]G. Wenz, "Acoustic ambient noise in the ocean, spectra and sources," J. Acoust. Soc. Am. **34**, 1936–1956 (1962).
[8]R. Francois and G. Garrison, "Sound absorption based on ocean measurements Part II: boric acid contribution and equation for total absorption," J. Acoust. Soc. Am. **72**, 1879–1890 (1982).
[9]R. Young, "Image interference in the presence of refraction," J. Acoust. Soc. Am. **19**, 1–7 (1947).